HEFAT2012
9th International Conference on Heat Transfer, Fluid Mechanics and Thermodynamics
16 – 18 July 2012
Malta

THERMAL INSTABILITY OF POISEUILLE-RAYLEIGH-BÉNARD FOR A SUPERCRITICAL FLUID IN A MINI-CHANNEL

Ameur D.* and Raspo I.
*Author for correspondence
M2P2, U.M.R. 7340 C.N.R.S.,
Aix-Marseille University,
Technopôle de Château-Gombert,
38 rue F. Joliot Curie, 13451 Marseille Cedex 20,
France,
E-mail: ameur@L3m.univ-mrs.fr

ABSTRACT

The Poiseuille-Rayleigh-Bénard (PRB) problem, involving the onset of thermoconvective structures in channels heated from below, was the subject of many theoretical, numerical and experimental studies for incompressible flows or perfect gas. However, to the authors' knowledge, this problem was never studied for supercritical fluids (SCF). The objective of this paper is to study the influence of the specific properties of SCF on thermoconvective instability phenomena compared with those observed in the perfect gas case. The effect of the distance to the critical point is also investigated. The numerical approach used is based on the Navier-Stokes equations in the framework of the low Mach number approximation.

INTRODUCTION

Poiseuille-Rayleigh-Bénard (PRB) flows are mixed convection flows in horizontal channels heated from below. When the Rayleigh number exceeds a critical value, thermoconvective structures develop in the channel. This paper focuses on these thermal instabilities in the case of fluids near their gas-liquid critical point. More precisely, a supercritical fluid (SCF) is a fluid for which temperature and pressure are larger than those of the critical point. In this zone of the phase diagram, the physical properties of the fluid (density, viscosity, diffusivity) are intermediate between those of liquids and gases. Moreover, they are very sensitive to temperature and pressure variations. These tunable properties motivated the use of SCF in many industrial applications, such as supercritical fluid extraction [1], particle generation [2], in particular in pharmaceutical industry, and preparation of metallic films using supercritical fluid deposition [3].

The instability onset and the development of the associated patterns in PRB flows were extensively studied for incompressible fluids and perfect gas from many years because the PRB configuration is relevant for several technological processes such as the cooling of microelectronic equipments [4] or the growth of thin crystal films from chemical vapor deposition (CVD) [5-8]. A detailed review of various studies reported in literature was performed by Nicolas in 2002 [9]. These studies showed that when the base flow becomes unstable, two kinds of thermoconvective structures may appear: transversal rolls at low Reynolds number (about $Re<10$) and longitudinal rolls at higher Reynolds number. The transversal rolls axes are perpendicular to the mean flow direction and these patterns can be considered as a quasi two-dimensional structure, whereas the longitudinal rolls axes are parallel to the mean flow and the three velocity components are excited. Results of linear stability analysis for incompressible flows showed that the transversal rolls are due to a convective or an absolute instability depending on the value of the Rayleigh number. The critical value of the two onsets depends on the Prandtl number and it increases with the Reynolds number. On the other hand, the longitudinal rolls can be only convectively unstable and the critical Rayleigh number is independent from the Reynolds and Prandtl numbers. These theoretical predictions were confirmed by experiments.

To the authors' knowledge, the PRB problem was never studied for fluids near their liquid-gas critical point while it is relevant for supercritical fluid deposition processes and it can be expected that the fluid response to the bottom boundary heating may be quite different in this special zone of the phase diagram. Indeed, as was already said, near the critical point, thermodynamic properties, such as density, and transport coefficients exhibit large variations with temperature and pressure. More precisely, on the critical isochore, several properties, such as isothermal compressibility, thermal expansion coefficient, specific heats or thermal conductivity, diverge as the critical temperature is approached, while other properties, such as thermal diffusivity, tend to zero. These critical behaviors cause some peculiar phenomena, such as a

fast heat transport by thermoacoustic effects (also called Piston effect) [10-12] in supercritical fluids. Natural convection in SCF was extensively studied in the past decade [13-23], especially in the Rayleigh-Bénard configuration [15-23]. These works showed, in particular, that the adiabatic temperature gradient, which is generally relevant only at large length scale, like for the study of atmospheric flows, must be taken into account for the convection onset in supercritical fluids in cavities of a few millimeters in height. We can therefore suppose that the specific properties of SCF may also modify the instability onset in the PRB configuration.

In the present paper, the stability of a supercritical fluid, modeled by the Peng-Robinson equation of state, in the PRB configuration is investigated using 2D direct numerical simulations. The first section is devoted to the mathematical formulation of the treated problem, namely the Navier-Stokes equations in the framework of the low Mach number approximation and the boundary conditions. Then, the numerical method, based on a Chebyshev collocation approximation, is described in details. Results obtained for a Reynolds number equal to 50.57 in a channel of height H'=1mm are presented in the third section. First, we studied the influence of the temperature increase on the onset and the development of convection for a fluid set at 1K above its critical temperature. The relation between the Rayleigh number and the instability characteristics is thus investigated. In a second part, we are focusing on the influence of the proximity to the critical point on the instability onset.

NOMENCLATURE

a	[-]	Energy parameter in the equation of state
b	[-]	Covolume in the equation of state
C_P'	[J/(kg.K)]	Isobaric specific heat
C_V'	[J/(kg.K)]	Isochoric specific heat
Fr	[-]	Froud number, $Fr = U_{ref}'^2 / (g'H')$
g'	[m/s^2]	Gravity constant
H'	[m]	Channel height
L'	[m]	Channel length
Ma	[-]	Mach number, $Ma = U_{ref}' / \sqrt{\gamma_0 R' T_c'}$
P'	[Pa]	pressure
Pr	[-]	Prandtl number, $Pr = C_P' \mu_b' / \lambda_b'$
R'	[J/(kg.K)]	Perfect gas constant
Ra	[-]	Rayleigh number, $Ra = \beta' g' \rho_c'^2 C_P' \delta T' H'^3 / (\mu_b' \lambda_b')$
Re	[-]	Reynolds number, $Re = \rho_c' U_{mean}' H' / \mu_b'$
t'	[s]	Time
T'	[K]	Temperature
u'	[m/s]	Velocity component in the x-direction
v'	[m/s]	Velocity component in the y-direction
x'	[m]	Cartesian axis direction
y'	[m]	Cartesian axis direction

Special characters

α	[-]	Soave function in the equation of state
β'	[K^{-1}]	Thermal expansion coefficient
δt	[-]	Dimensionless time step
$\delta T'$	[K]	Temperature increase
ε	[-]	Dimensionless proximity to the critical point, $\varepsilon = (T_i' - T_c')/T_c'$
λ'	[W/(m.K)]	Thermal conductivity
μ'	[Pa.s]	Dynamic viscosity
ρ'	[kg/m^3]	Density
χ'	[Pa^{-1}]	Isothermal compressibility
ω	[-]	Acentric factor
Ω	[-]	Computational domain
$\partial\Omega$	[-]	Boundary of the computational domain
γ	[-]	Specific heats ratio

Subscripts

b	Background property
c	Critical property
dyn	Dynamic part
hyd	Hydrostatic part
i	Initial value
$mean$	Mean value
ref	Reference value
th	Thermodynamic part
0	Value for the perfect gas

PHYSICAL PROBLEM AND MODELLING

The physical model consists of a 2D channel of height H'=1mm, with an aspect ratio L'/H'=10 or 15. The carried fluid is supercritical CO_2 subject to gravity. Initially, the fluid is at a uniform temperature slightly above the critical temperature, $T_i'=(1+\varepsilon)T_c'$ (with ε<<1), and at a mean density equal to the critical density ρ_c', and it flows through the channel according to a Poiseuille profile. Then, the temperature of the bottom wall is gradually increased up to $T_{ch}'=T_i'+\delta T'$ (with $\delta T'$ ranging from about ten to some hundreds milliKelvin) from a distance H' from inlet (cf. Figure 1).

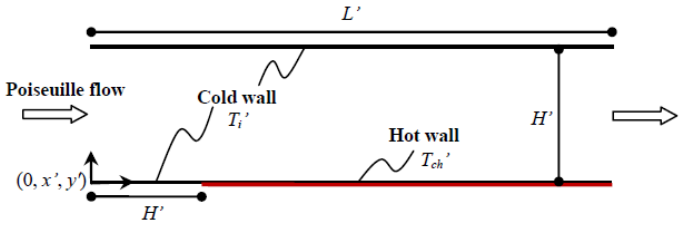

Figure 1 Channel geometry with top and bottom thermal boundary conditions.

The supercritical fluid is modeled by the Peng-Robinson equation of state. This equation implicitly accounts for the divergence of the thermal expansion coefficient β' of the isothermal compressibility χ' and of the specific heat at constant pressure C_P' near the liquid-gas critical point. The divergence of the thermal conductivity λ' is modelled by the formula $\lambda' = \lambda_b'[1+\Lambda(T'/T_c'-1)^{-0.5}]$. The physical parameters of CO_2 were used: T_c'=304.13K, ρ_c'=467.8kg.m^{-3}, λ_b'=0.04412W.m^{-1}.K^{-1}, Λ=0.75.

The evolution of the flow is governed by the time-dependent 2D Navier-Stokes equations coupled with the energy and the Peng-Robinson equations. These equations are solved in the framework of the low Mach number approximation [24]: the pressure P' is thus split into a thermodynamic part, P_{th}', which is constant in space and appears in the energy equation

and the equation of state, and a dynamic part, P_{dyn}', involved in the momentum equation. However, the basic approximation of Paolucci [24] is modified as proposed in [25] to account for the stratification of the fluid near the critical point since Ma^2/Fr (where Ma and Fr are respectively the Mach and the Froud numbers) is not in O(Ma^2). We chose as characteristic variables T_c' for temperature, ρ_c' for density, $\rho_c' R' T_c'$ for pressure (with R'=188.92J.kg^{-1}.K^{-1} the perfect gas constant), H' for length, $U'_{ref} = \sqrt{\beta' g' \delta T' H'}$ for velocity (with g' the Earth gravity), H'/U'_{ref} for time and λ_b' for the thermal conductivity. The specific heat at constant volume C_V' and the dynamic viscosity μ' were fixed to their background values, C_{Vb}'=472.313J.kg^{-1}.K^{-1} and μ_b'=3.2702×10^{-5}Pa.s. The dimensionless governing equations are therefore:

$$\frac{\partial \rho}{\partial t} + \nabla.(\rho \mathbf{V}) = 0 \tag{1}$$

$$\rho \frac{\partial \mathbf{V}}{\partial t} + \rho \mathbf{V}.\nabla \mathbf{V} = -\nabla P_{dyn} + \sqrt{\frac{Pr}{Ra}} \left[\Delta \mathbf{V} + \frac{1}{3} \nabla (\nabla.\mathbf{V}) \right] - \frac{1}{Fr} (\rho - \rho_i) \mathbf{e}_y \tag{2}$$

$$\rho \frac{\partial T}{\partial t} + \rho \mathbf{V}.\nabla T = -(\gamma_0 - 1) T \left(\frac{\partial P}{\partial T} \right)_\rho (\nabla.\mathbf{V}) + \frac{\gamma_0}{Pr_0} \sqrt{\frac{Pr}{Ra}} \nabla.(\lambda \nabla T) \tag{3}$$

$$P_{th} + P_{hyd} = \frac{\rho T}{1 - b\rho} - \frac{a\, \alpha(T) \rho^2}{1 + 2b\rho - b^2 \rho^2} \tag{4}$$

with a and b the dimensionless energy parameter and covolume respectively and α the Soave function defined by:

$$a = 1.487422 \ , b = 0.253076 \ , \ \alpha(T) = \left[1 + m\left(1 - \sqrt{T}\right) \right]^2$$

where m is computed from the acentric factor ω (ω=0.225 for CO_2) by the formula $m = 0.37464 + 1.54226\omega - 0.26992\omega^2$.

In Eqs. (1)-(4), P_{hyd} is the hydrostatic pressure introduced by the modification of the Low Mach number approximation, $\mathbf{e}_y$ is the unit vector in the y-direction and γ_0 and Pr_0 are respectively the specific heats ratio and the Prandtl number for the perfect gas (γ_0=1.4, Pr_0=0.6567). The other dimensionless numbers introduced are the Prandtl number Pr, the Rayleigh number Ra, the Mach number Ma and the Froud number Fr which are defined by:

$$Pr = \frac{C_P' \mu_b'}{\lambda_b'} \ , Ra = \frac{\beta' g' \rho_c'^2 C_P' \delta T' H'^3}{\mu_b' \lambda_b'} \ , Ma = \frac{U'_{ref}}{\sqrt{\gamma_0 R' T_c'}} \ , Fr = \frac{U'^2_{ref}}{g' H'}$$

In the above formula, the physical parameters β' and C_P' are calculated for the initial state (T_i', ρ_i') from the equation of state. The initial condition for the dimensionless variables in Ω=[0,L'/H']×[0,1] is:

$$u_i(x,y) = 1.5Re\sqrt{\frac{Pr}{Ra}}\left[1-(2y-1)^2\right] \ , \ v_i(x,y) = 0 \tag{5}$$

where Re is the Reynolds number defined by $Re = \rho_c' U'_{mean} H' / \mu_b'$, with U'_{mean} the mean velocity at inlet,

$$T_i(x,y) = 1 + \varepsilon \tag{6}$$

and, as it was proposed in [25], the stratification of the fluid is taken into account leading to the initial condition for density and pressure:

$$\rho_i(x,y) = K_2 \frac{e^{-K_2 y}}{1 - e^{-K_2}} \tag{7}$$

$$P_i(x,y) = P_{thi} + P_{hyd}(y) \tag{8}$$

with $K_2 = \gamma_0 \dfrac{Ma^2}{K_1 Fr}$, $K_1 = \dfrac{1+\varepsilon}{(1-b)^2} - \dfrac{2(1+b)\alpha(T_i)}{\left(1+2b-b^2\right)^2}$

and:

$$P_{thi} = \frac{1+\varepsilon}{1-b} - \frac{\alpha(T_i)}{1+2b-b^2} \ , \ P_{hyd}(y) = K_1 \left[K_2 \frac{e^{-K_2 y}}{1 - e^{-K_2}} - 1 \right]$$

Equations (1)-(4) are solved with the following boundary conditions:

- On the channel walls, the no-slip condition is prescribed for the velocity. The top wall (y=1) is kept at the initial temperature T_i. On the bottom heated wall (y=0), in order to avoid a discontinuity of the temperature profile. the following boundary condition is imposed for 0≤x≤L'/H':

$$T(x) = T_i + \delta T \left[th(2x-2) - th(-2) \right] / \left[th(18) - th(-2) \right] \tag{9}$$

This boundary condition allows a continuous transition between the cold entry zone for 0≤ x≤1 and the hot zone for 1≤ x≤L'/H'.

- At the channel inlet (x=0), temperature is kept at its initial value T_i and a parabolic profile is imposed for velocity:

$$T(y) = T_i = 1 + \varepsilon$$
$$u(y) = 1.5Re\sqrt{\frac{Pr}{Ra}}\left[1-(2y-1)^2\right] \ , \ v(y) = 0 \tag{10}$$

- At the channel outlet (x=L'/H'), an Orlanski type boundary condition is prescribed for all the variables:

$$\frac{\partial \phi}{\partial t} + Re\sqrt{\frac{Pr}{Ra}} \frac{\partial \phi}{\partial x} = 0 \quad \text{for} \quad \phi = T, u, v. \tag{11}$$

NUMERICAL METHOD

Time scheme and space approximation

Equations (1)-(4) are discretized in time with a second order semi-implicit scheme: the convective terms are evaluated by an Adams-Bashforth scheme, a second order backward Euler scheme is used for the discretization of time derivatives and the diffusive terms as the energy source term $-T(\partial P/\partial T)_\rho (\nabla.\mathbf{V})$

are implicitly treated. The outlet boundary condition (11) is also discretized using the same second order scheme, leading to a Dirichlet boundary condition for the variables at the current time step *n+1*.

The space approximation is performed using a Chebyshev-collocation method with Gauss-Lobatto points. For the computation of the convective terms, the derivatives are calculated in the spectral space and the products are performed in the physical one; the connection between the spectral and the physical spaces is realized through a FFT algorithm. On the other hand, the spectral differentiation matrices are used for the derivatives in the diffusive terms.

Numerical algorithm

At a given time step, the discretized equations are coupled because of the implicit treatment of the energy source term involving $\nabla.\mathbf{V}$. This term must be implicitly evaluated for supercritical fluids. However, it is possible to completely uncouple the solution of the energy equation and the computation of the dynamic field by calculating the velocity divergence from the sole knowledge of the thermodynamic variables [26, 27]. The procedure consists in taking the total derivative of the equation of state (4) written in the form $F(P_{th},T,\rho)=0$. Then, using the energy equation (3) and the continuity equation (1), the following formula is obtained for the velocity divergence:

$$\nabla.\mathbf{V} = \frac{\dfrac{dP_{th}}{dt} + \dfrac{\gamma_0}{Pr_0}\sqrt{\dfrac{Pr}{Ra}}\dfrac{1}{\rho}\left(\dfrac{\partial F}{\partial T}\right)_{\rho,P_{th}}\nabla.(\lambda\nabla T)}{\rho\left(\dfrac{\partial F}{\partial \rho}\right)_{T,P_{th}} + (\gamma_0-1)\dfrac{T}{\rho}\left(\dfrac{\partial P_{th}}{\partial T}\right)_{\rho}\left(\dfrac{\partial F}{\partial T}\right)_{\rho,P_{th}}} \qquad (12)$$

with: $$\frac{1}{\rho}\left(\frac{\partial F}{\partial T}\right)_{\rho,P_{th}} = -\frac{1}{1-b\rho} + \frac{a\rho}{1+2b\rho-b^2\rho^2}\frac{d\alpha}{dT}$$

$$\left(\frac{\partial F}{\partial \rho}\right)_{T,P_{th}} = -\frac{T}{(1-b\rho)^2} + \frac{2a\,\alpha(T)(1+b\rho)\rho^2}{(1+2b\rho-b^2\rho^2)^2}$$

$$T\left(\frac{\partial P_{th}}{\partial T}\right)_{\rho} = P_{th} + P_{hyd} - a\left(T\frac{d\alpha}{dT}-\alpha\right)\frac{\rho^2}{1+2b\rho-b^2\rho^2}$$

In the case of an open system, as the one considered here, the thermodynamic pressure P_{th} is also constant in time. Therefore, the time derivative dP_{th}/dt disappears in Eq. (12). Otherwise, this derivative can be evaluated using a second order backward Euler scheme as in [27].

Thanks to Eq. (12), the discretized equations are solved in two successive steps: first, the thermodynamic variables are computed through an iterative algorithm [26, 27] and then the Navier-Stokes equations are solved using the modified projection method developed in [28] and extended to variable density flows. The two steps are described in details below.

<u>- 1st step: Computation of (T, ρ, $\nabla.\mathbf{V}$)</u>

At time step *n+1*, the discretized energy equation can be written as a Helmholtz equation with coefficients involving λ^{n+1} and ρ^{n+1}. In order to take advantage of the efficiency of the full diagonalization technique developed for the solution of Helmholtz problems with time-independent coefficients [29], the density and the thermal conductivity are split into a constant part, namely their value at t=0, and a time-dependent part. So, the terms involving the time-dependent parts are treated as source terms and the discretized energy equation can be written as a Helmholtz equation with constant coefficients. The complete diagonalization of the Helmholtz operator with constant coefficients is performed once for all in a preprocessing stage. Then, at each time step, the solution of the Helmholtz problem is reduced to matrix products, leading to a very efficient solution technique on supercomputers.

More precisely, the computation of T, ρ and $\nabla.\mathbf{V}$ is performed through the following iterative algorithm:

1. The variables T^{k-1}, ρ^{k-1} and $(\nabla.\mathbf{V})^{k-1}$ are initialized at their values at the previous time step *n;*
2. The temperature T^k is obtained by the solution of the Helmholtz equation:

$$\frac{\gamma_0}{Pr_0}\sqrt{\frac{Pr}{Ra}}\lambda_i\Delta T^k - \frac{3}{2\delta t}\rho_i T^k = \left(\rho^{k-1}-\rho_i\right)\frac{3\,T^{k-1}}{2\delta t} - \frac{\gamma_0}{Pr_0}\sqrt{\frac{Pr}{Ra}}\nabla.\left(\left(\lambda^{k-1}-\lambda_i\right)\nabla T^{k-1}\right) + (\gamma_0-1)T^{k-1}\left(\frac{\partial P_{th}}{\partial T}\right)_{\rho}^{k-1}(\nabla.V)^{k-1} - \rho^{k-1}\left(\frac{4T^n - T^{n-1}}{2\delta t}\right) + AB\left(\rho\mathbf{V}.\nabla T\right)^{n,n-1}$$

   with the boundary conditions of the problem. In the above equation, δt is the time-step and the notation *AB(.)* means an Adams-Bashforth evaluation of the quantity:

$$AB(\phi)^{n,n-1} = 2\phi^n - \phi^{n-1}$$

3. The thermal conductivity λ^k is updated;
4. The density ρ^k is computed from the equation of state (4);
5. The velocity divergence $(\nabla.\mathbf{V})^k$ is computed by Eq. (12).

The steps 2 to 5 are repeated until convergence is achieved on temperature and density. The convergence criterion used is $\mathrm{Max}(Res T, Res\rho)<10^{-11}$, with $Res\phi=\mathrm{Max}((\phi^k-\phi^{k-1})/\phi^{k-1})$ for $\phi=T,\rho$ and the maximum number of iterations is fixed to 150.

<u>- 2nd step: Computation of ($\mathbf{V}$, P_{dyn})</u>

When starting the solution of the Navier-Stokes equations, temperature, density and velocity divergence at the current time step *(n+1)* are known. It is therefore possible to use a projection-type algorithm such as those developed for the solution of incompressible Navier-Stokes equations, with some modifications. In this work, we have used the modified projection method proposed by Hugues and Randriamampianina [28] and analysed in details in [30]. It was

shown in particular that the modification introduced by Hugues and Randriamampianina, namely the computation of a preliminary pressure, improves the accuracy on pressure and allows to reduce the slip velocity compared to other projection methods [30]. The modified projection method consists in solving the Navier-Stokes equations by three successive steps as follows:

- *Computation of a preliminary pressure*

First, a preliminary pressure $\bar{P}_{dyn}^{n+1}$ is computed from a Poisson equation derived from the discretized momentum equation (2):

$$\Delta\bar{P}_{dyn}^{n+1} = \nabla.\left[-AB\left(\rho\mathbf{V}.\nabla\mathbf{V}\right)^{n,n-1} + \rho^{n+1}\left(\frac{4\mathbf{V}^n - \mathbf{V}^{n-1}}{2\delta t}\right) + \frac{1}{3}\sqrt{\frac{Pr}{Ra}}\nabla\left(\nabla.\mathbf{V}\right)^{n+1} - \frac{1}{Fr}\left(\rho^{n+1} - \rho_i\right)\mathbf{e}_y \right] + \sqrt{\frac{Pr}{Ra}}\Delta\left(\nabla.\mathbf{V}\right)^{n+1} + \frac{3}{2\delta t}\left(\frac{3\rho^{n+1} - 4\rho^n + \rho^{n-1}}{2\delta t}\right)$$

Neumann boundary conditions are obtained by the normal projection of the momentum equation (2) on the boundary:

$$\frac{\partial\bar{P}_{dyn}^{n+1}}{\partial n} = n.\left[-AB\left(\rho\mathbf{V}.\nabla\mathbf{V}\right)^{n,n-1} + \rho^{n+1}\left(\frac{-3\mathbf{W}^{n+1} + 4\mathbf{V}^n - \mathbf{V}^{n-1}}{2\delta t}\right) + \frac{4}{3}\sqrt{\frac{Pr}{Ra}}\nabla\left(\nabla.\mathbf{V}\right)^{n+1} - \frac{1}{Fr}\left(\rho^{n+1} - \rho_i\right)\mathbf{e}_y - \sqrt{\frac{Pr}{Ra}}AB\left(\nabla\times\left(\nabla\times\mathbf{V}\right)\right)^{n,n-1} \right]$$

where $\mathbf{W}^{n+1}$ represents the velocity boundary condition. At the channel outlet, the discretization of Eq. (11) leads to:

$$\mathbf{W}^{n+1} = \frac{2\delta t}{3}\left[\frac{4\mathbf{V}^n - \mathbf{V}^{n-1}}{2\delta t} - Re\sqrt{\frac{Pr}{Ra}}AB\left(\frac{\partial\mathbf{V}}{\partial x}\right)^{n,n-1} \right]$$

- *Computation of a predicted velocity* $\mathbf{V}^*$

The predicted velocity field $\mathbf{V}^*$ is computed implicitly from the momentum equation with the gradient of the preliminary pressure instead of that of the actual pressure P_{dyn}^{n+1}. The predicted velocity therefore satisfies the following problem:

$$\begin{cases} \rho^{n+1}\dfrac{3\mathbf{V}^* - 4\mathbf{V}^n + \mathbf{V}^{n-1}}{2\delta t} + AB\left(\rho\mathbf{V}.\nabla\mathbf{V}\right)^{n,n-1} \\ \qquad = -\nabla\bar{P}_{dyn}^{n+1} + \sqrt{\dfrac{Pr}{Ra}}\Delta\mathbf{V}^* \\ \qquad + \dfrac{1}{3}\sqrt{\dfrac{Pr}{Ra}}\nabla\left(\nabla.\mathbf{V}\right)^{n+1} \\ \qquad - \dfrac{1}{Fr}\left(\rho^{n+1} - \rho_i\right)\mathbf{e}_y \qquad \text{in } \Omega \\ \mathbf{V}^* = \mathbf{W}^{n+1} \qquad \text{on } \partial\Omega \end{cases}$$

Here again, we have to solve Helmholtz equations with coefficients involving ρ^{n+1} for each velocity component. As for the energy equation, the density ρ^{n+1} is split into a constant part and a time-dependent part and Helmholtz equations with constant coefficients are solved iteratively for each velocity component. The convergence is achieved when Max*(Resu, Resv)*<10^{-13}. This criterion is fulfilled after 3 or 4 iterations.

- *Correction step*

The converged velocity field $\mathbf{V}^*$ is then corrected by taking into account the pressure gradient at the current time step (*n+1*) so that the final velocity field satisfies the continuity equation (1). This correction is performed through the solution of the following Poisson problem for the intermediate variable $\varphi = 2\delta t\left(P_{dyn}^{n+1} - \bar{P}_{dyn}^{n+1}\right)/3$:

$$\begin{cases} \Delta\varphi = \nabla.\left(\rho^{n+1}\mathbf{V}^*\right) + \dfrac{3\rho^{n+1} - 4\rho^n + \rho^{n-1}}{2\delta t} & \text{in } \Omega \\ \dfrac{\partial\varphi}{\partial n} = 0 & \text{on } \partial\Omega \end{cases}$$

It must be noted that the above Poisson-Neumann problem must fulfill a compatibility condition to be solvable. Because of the inhomogeneous Dirichlet condition for the predicted velocity $\mathbf{V}^*$ at the channel outlet, this compatibility condition is not fulfilled. A renormalization of $\mathbf{V}^*$ at the outlet boundary was therefore performed before the solution of the Poisson-Neumann problem as proposed in [31].

The actual velocity field and pressure at the current time step (*n+1*) are finally calculated in $\Omega\cup\partial\Omega$ by the formulae:

$$\mathbf{V}^{n+1} = \mathbf{V}^* - \frac{1}{\rho^{n+1}}\nabla\varphi \ , \ P_{dyn}^{n+1} = \bar{P}_{dyn}^{n+1} + \frac{3}{2\delta t}\varphi \ .$$

RESULTS AND DISCUSSION

Simulations were performed for a Reynolds number *Re*=50.57. Instantaneous temperature fields at several times are presented in order to show the spatio-temporal evolution of the thermoconvective structures. First, the fluid was set at 1K above its critical temperature, which corresponds to a dimensionless distance to the critical point $\varepsilon=3.288\times10^{-3}$, and several values of the bottom wall heating were considered. These results were obtained in a channel with an aspect ratio *L'/H'*=10. Then, the influence of the proximity to the critical point was investigated. In this case, in order to track further the different structures in the channel, we increased the aspect ratio to *L'/H'*=15.

Thermoconvective instabilities at 1K from the critical point

Computations were carried out for $\delta T'$ ranging from 2×10^{-2}K up to 10^{-1}K. Because of the divergence of the thermal expansion coefficient β' and of the isobaric specific heat C_p' near the critical point, these small temperature increases induce large Rayleigh numbers ranging from 1.05×10^6 to 5.23×10^6 . Figure 2 shows the temperature fields for several values of $\delta T'$

collected at different calculation times. In all the cases, instability appears in the form of thermal plumes which develop on the hot boundary layer. These structures are similar to those previously obtained for a supercritical fluid in the Rayleigh-Bénard configuration [14-22]. However, in a closed cavity, the bottom wall heating induces a piston effect that homogeneously increases the bulk temperature and gives rise to a second unstable thermal boundary layer on the top cold wall. This is not the case in an open channel as it can be seen in Figure 2. The couple (t'_{ins}, x'_{ins}) (where t'_{ins} is the time corresponding to the beginning of the isotherms deformation and x'_{ins} the axial position of the first plume) which characterizes the instability onset is respectively (4*H'*, 1.22s), (3*H'*, 0.71s), (1*H'*, 0.33s) for $\delta T'$=2×10^{-2}K, 4×10^{-2}K and 10^{-1}K. So the thermoconvective instability appears earlier and closer to the beginning of the heated zone when the Rayleigh number is increased. Furthermore, as the heating increases, the disturbances grow faster.

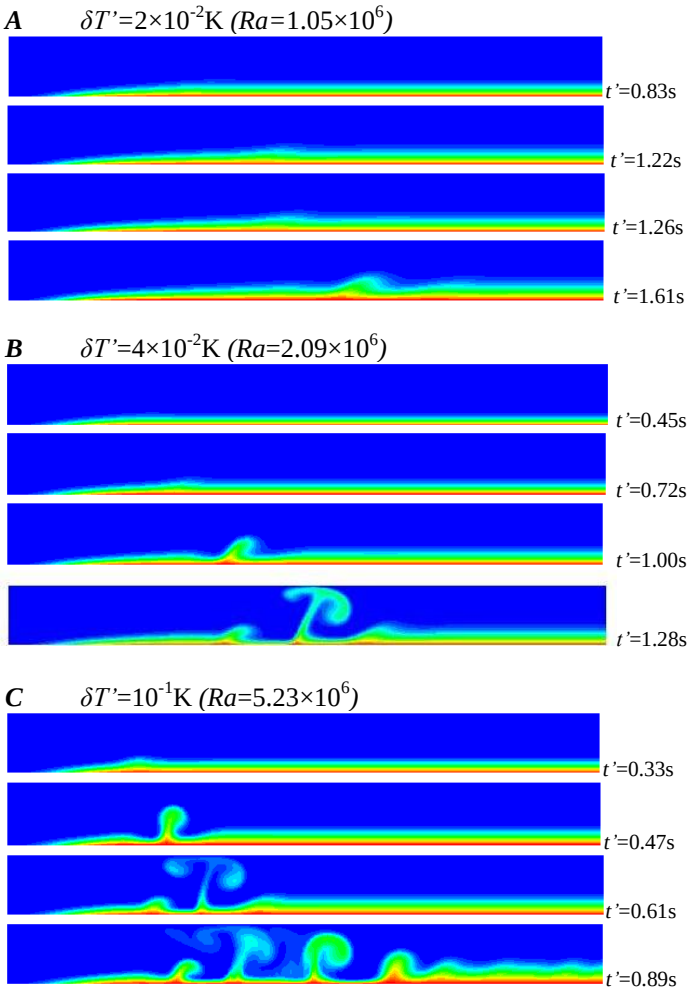

Figure 2 Temperature field for $T_i' = T_c'$+1K (*Pr* =31.72).

Figure 2 also shows that the number and the development of the thermoconvective structures are different according to the value of $\delta T'$. While instability appears in the form of one or some plumes which move downstream during time for $\delta T'$ about 10^{-2}K (cases A and B), many structures develop in the whole channel for the largest heating (case C). In addition, in this last case, as the structures move downstream, new thermal plumes continuously appear near the beginning of the heated zone. According to previous studies [32], the time evolution of the patterns may indicate that the structures are due to a convective instability in cases A and B and to an absolute instability in case C. As a consequence, since longitudinal rolls can never be absolutely unstable, as it was shown in [32], the thermoconvective structures in Figure 2 could be transversal rolls. Further simulations are necessary to confirm this assumption. However, if these results were confirmed, they would indicate that the transition between transversal rolls and longitudinal rolls occurs for larger Reynolds number values than for perfect gas or incompressible fluids.

Influence of the distance to the critical point on the thermoconvective instabilities

Very close to the critical point, several physical properties, such as thermal expansion coefficient and isobaric specific heat, diverge. In order to study the influence of these diverging properties on the stability of the supercritical fluid, simulations were performed at 5K from the critical temperature. In this case, the dimensionless distance to the critical point is ε=1.644×10^{-2}.

$T_i' - T_c'$ (K)	β' (K^{-1})	C_p' (J/kg/K)	*Pr*
1	0.82199	42803.48	31.72
5	0.15334	8478.77	6.28

Table 1 Thermodynamic properties and Prandtl number at 1K and 5K to the critical point.

As is shown in Table 1, the thermal expansion coefficient and the isobaric specific heat strongly decrease as the distance to the critical point increases. As a consequence, Rayleigh numbers obtained for similar temperature differences $\delta T'$ are much smaller than those involved at 1K from T_c'. In addition, the Prandtl number *Pr* at 5K from the critical point is 5 times smaller than at 1K. This change of *Pr* is quite significant and previous studies for incompressible fluids or perfect gas showed that the critical Rayleigh number depends (respectively does not depend) on *Pr* for the onset of transversal rolls (respectively longitudinal rolls) [32].

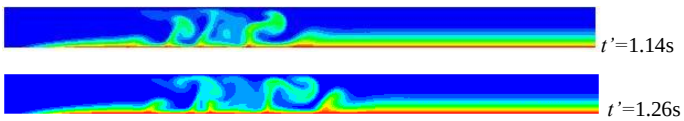

Figure 3 Temperature field for $T_i' = T_c'$+5K (*Pr* =6.28) and *Ra*=5.23×10^5.

Figure 3 shows the temperature fields obtained for a temperature increase $\delta T'=2.7\times10^{-1}$K, corresponding to a Rayleigh number $Ra=5.23\times10^5$. The Rayleigh number is therefore smaller than the smallest value that we considered at 1K from T_c' (case A). It can be noted that the thermoconvective structures develop much faster compared to case A of Figure 2 and they are also much larger. This fast and strong growth of the perturbations means that $Ra=5.23\times10^5$ is much larger than the critical value for the instability threshold. Therefore, these results reveal that, for $Re=50.57$, the critical Rayleigh number is smaller at 5K than at 1K from the critical point and, consequently, it means that it depends on the Prandtl number. According to the previous studies [32], this result confirms that the observed thermoconvective structures may be transversal rolls.

CONCLUSION

In this paper, the Poiseuille-Rayleigh-Bénard problem for a supercritical fluid, modeled by the Peng-Robinson equation of state, was studied for a Reynolds number $Re=50.57$. The temperature fields obtained in a channel of height $H'=1$mm revealed the existence of thermoconvective instabilities appearing in the form of thermal plumes, similar to those previously observed in supercritical fluids in the Rayleigh-Bénard configuration [14-22]. These thermal plumes develop on the hot boundary layer and then move downstream during time. Thus, contrary to the perfect gas case, for which the convective structures occupy the whole height of the channel, instability develops here on the fine thermal boundary layer along the heated zone. The temporal evolution of the patterns indicates that the instability is convective or absolute depending on the value of the Rayleigh number. As a consequence, since longitudinal rolls can never be absolutely unstable [32], the thermoconvective structures could be transversal rolls.

Moreover, the results obtained at different distances from the critical point showed that the critical Rayleigh number for the first instability threshold depends on the Prandtl number. This variation of the critical Rayleigh number with the Prandtl number is also characteristic of transversal rolls according to previous studies [32].

Obviously, the results presented here are preliminary results and further simulations are necessary to confirm the type of structures that we obtained. In particular, simulations will be performed to determine the convective instability threshold for various values of the Reynolds number as well as the Reynolds number for the transition between transversal rolls and longitudinal rolls. Three-dimensional computations will also be carried out.

Acknowledgements.

The authors acknowledge the french 'Agence Nationale de la Recherche' (ANR) for its financial support (2009 White Program ANR-09-BLAN-0105-01). This work was performed using HPC resources from GENCI-IDRIS (grants 2011-20321 and 2012-20321).

REFERENCES

[1] Reverchon E. and De Marco I., Supercritical fluid extraction and fractionation of natural matter, *Journal of Supercritical Fluids*, Vol. 38, 2006, pp. 146-166.

[2] Cocero M. J., Martin A., Mattea F. and Varona S., Encapsulation and co-precipitation processes with supercritical fluids: fundamentals and applications, *Journal of Supercritical Fluids*, Vol. 47, 2009, pp. 546-555.

[3] Erkey C., Preparation of metallic supported nanoparticles and films using supercritical fluid deposition, *Journal of Supercritical Fluid*, Vol. 47, 2009, pp. 517-522.

[4] Incropera F. P., Convective heat transfer in electronic equipment cooling, *Journal of Heat Transfer*, Vol. 110, 1988, pp.1097-1111.

[5] Evans G. and Greif R., A study of traveling wave instabilities in a horizontal channel flow with applications to chemical vapor deposition, *International Journal of Heat and Mass Transfer*, Vol. 32, 1989, pp. 895-911.

[6] Evans G. and Greif R., Unsteady three-dimensional mixed convection in a heated horizontal channel with applications to chemical vapor deposition, *International Journal of Heat and Mass Transfer*, Vol. 34, 1991, pp. 2039-2051.

[7] Evans G. and Greif R., Thermally unstable convection with applications to chemical vapor deposition channel reactors, *International Journal of Heat and Mass Transfer*, Vol. 36, 1993, pp. 2769-

[8] Spall R. E., Unsteady mixed convection in horizontal ducts with applications to chemical vapor deposition processes, *International Communications in Heat and Mass Transfer*, Vol. 23, 1996, pp. 115-122.

[9] Nicolas X., Bibliographical review on the Poiseuille–Rayleigh–Bénard flows: the mixed convection flows in horizontal rectangular ducts heated from below, *International Journal of Thermal Science*, Vol. 41, 2002, pp. 961-1016.

[10] Onuki A., Hao H. and Ferrell R. A., Fast adiabatic equilibration in a single-component fluid near the liquid-vapor critical point, *Physical Review A*, Vol. 41, 1990, pp. 2256-2259.

[11] Boukari H., Shaumeyer J. N., Briggs M. E. and Gammon, R. W., Critical speeding up in pure fluids, *Physical Review A*, Vol. 41, 1990, pp. 2260-2263.

[12] Zappoli B., Bailly D., Garrabos Y., Le Neindre B., Guenoun P., and Beysens D., Anomalous heat transport by the piston effect in supercritical fluids under zero gravity, *Physical Review A*, Vol. 41, 1990, pp. 2264-2267.

[13] Zappoli B., Amiroudine S., Carlès P. and Ouazzani J., Thermoacoustic and buoyancy-driven transport in a square side-heated cavity filled with a near-critical fluid, *Journal of Fluid Mechanics*, Vol. 316, 1996, pp. 53-72.

[14] Chiwata Y. and Onuki A., Thermal plumes and convection in highly compressible fluids, *Physical Review Letters*, Vol. 87, 2001, pp. 144301.

[15] Amiroudine S., Bontoux P., Larroudé P., Gilly B. and Zappoli B., Direct numerical simulation of instabilities in a two-dimensional near-critical fluid layer heated from below, *Journal of Fluid Mechanics*, Vol. 442, 2001, pp. 119-140.

[16] Furukawa A. and Onuki A., Convective heat transport in compressible fluids, *Physical Review E*, Vol. 66, 2002, pp. 016302.

[17] Furukawa A., Meyer H., Onuki A. and Kogan A. B., Convection in a very compressible fluid: comparison of simulations with experiments, *Physical Review E*, Vol. 68, 2003, pp. 56301–56309.

[18] Amiroudine S. and Zappoli B., Piston-effect-induced thermal oscillations at the Rayleigh-Bénard threshold in supercritical He, *Physical Review Letters*, Vol. 90, 2003, pp. 105301–105303.

[19] Raspo I., Zappoli B. and Bontoux P., Unsteady two-dimensional convection in a bottom heated supercritical fluid, *Comptes Rendus de Mécanique*, Vol. 332, 2004, pp. 353-360.
[20] Accary G., Raspo I., Bontoux P. and Zappoli B., Three-dimensional Rayleigh-Bénard instability in a supercritical fluid, *Comptes Rendus de Mécanique*, Vol. 332, 2004, pp. 209-216.
[21] Accary G., Raspo I., Bontoux P. and Zappoli B., Reverse transition to hydrodynamic stability through the Schwarzschild line in a supercritical fluid layer, *Physical Review E*, Vol. 72, 2005, pp. 035301.
[22] Accary G., Raspo I., Bontoux P. and Zappoli B., Stability of a supercritical fluid diffusing layer with mixed boundary conditions', *Physics of Fluids*, Vol. 17, 2005, p. 104105.
[23] Gorbunov A. A., Nikitin S. A. and Polezhaev V., Conditions of Rayleigh-Bénard convection onset and heat transfer in a near-critical medium, *Fluid Dynamics*, Vol. 42, 2007, pp. 704-718.
[24] Paolucci S., On the filtering of sound from the Navier-Stokes equations, *Technical report, Sandia National Laboratories USA, SAND82-8257*, 1982.
[25] Accary G., Raspo I. B,ontoux P., and Zappoli B., An adaptation of the low Mach number approximation for supercritical fluid buoyant flows, *Comptes Rendus de Mécanique*, Vol. 333, 2005, pp. 397-404.
[26] Ouazzani J. and Garrabos Y. A new numerical algorithm for low Mach number supercritical fluids, (available at https://hal.archives-ouvertes.fr/hal-00142988).
[27] Raspo I. and Ouazzani J., Un algorithme faible nombre de Mach pour la simulation des écoulements de fluides supercritiques par des méthodes spectrales, *Proceedings of the XIXème Congrès Français de Mécanique*, C Rey, P. Bontoux, A. Chrysochoos Eds., ISSN 2103_6225, paper 337-S05, 2009.
[28] Hugues S. and Randriamampianina A., An improved projection scheme applied to pseudospectral methods for the incompressible Navier-Stokes equations, *International Journal for Numerical Methods in Fluids*, Vol. 28, 1998, pp. 501-521.
[29] Haldenwang P., Labrosse G., Abboudi S. and Deville M., Chebyshev 3D spectral and 2D pseudospectral solvers for the Helmholtz equation, *Journal of Computional Physics*, Vol. 55, 1984, pp. 115-128.
[30] Raspo I., Hugues S., Serre E., Randriamampianina A. and Bontoux P., A spectral projection method for the simulation of complex three - dimensional rotating flows, *Computers and Fluids*, Vol. 31, 2002, pp. 745-767.
[31] Le H. and Moin P., Direct numerical simulation of turbulent flow over a backward-facing step, *Report TF-58, Thermosciences Division, Dept. of Mech. Eng. Stanford University*, 1994.
[32] Carrière P. and Monkewitz P. A., Convective versus absolute instability in mixed Rayleigh-Bénard-Poiseuille convection, *Journal of Fluid Mechanics*, Vol. 384, 1999, pp. 243-262.